ACS APPLIED MATERIALS & INTERFACES

Research Article

www.acsami.org

Water-Soluble Pd Nanoparticles Synthesized from ω-Carboxyl-*S*-Alkanethiosulfate Ligand Precursors as Unimolecular Micelle Catalysts

Diego J. Gavia, May S. Maung, and Young-Seok Shon*

Department of Chemistry and Biochemistry, California State University, Long Beach, 1250 Bellflower Boulevard, Long Beach, California 90840, United States

Supporting Information

ABSTRACT: This report describes a two-phase synthesis of water-soluble carboxylate-functionalized alkanethiolate-capped Pd nanoparticles from ω-carboxyl-*S*-alkanethiosulfate sodium salts. The two-phase methodology using the thiosulfate ligand passivation protocol allowed a highly specific control over the surface ligand coverage of these nanoparticles, which are lost in a one-phase aqueous system because of the base-catalyzed hydrolysis of thiosulfate to thiolate. Systematic synthetic variations investigated in this study included the concentration of ω-carboxyl-*S*-alkanethiosulfate ligand precursors and reducing agent, $NaBH_4$, and the overall ligand chain length. The resulting water-soluble Pd nanoparticles were isolated and characterized by transmission electron microscopy (TEM), thermogravimetric analysis (TGA), ^1H NMR, UV−vis, and FT-IR spectroscopy. Among different variations, a decrease in the molar equivalent of $NaBH_4$ resulted in a reduction in the surface ligand density while maintaining a similar particle core size. Additionally, reducing the chain length of the thiosulfate ligand precursor also led to the formation of stable nanoparticles with a lower surface coverage. Since the metal core size of these Pd nanoparticle variations remained quite consistent, direct correlation studies between ligand properties and catalytic activities against hydrogenation/isomerization of allyl alcohol could be performed. Briefly, Pd nanoparticles dissolved in water favored the hydrogenation of allyl alcohol to 1-propanol whereas Pd nanoparticles heterogeneously dispersed in chloroform exhibited a rather high selectivity towards the isomerization product (propanal). The results suggested that the surrounding ligand environments, such as the ligand structure, conformation, and surface coverage, were crucial in determining the overall activity and selectivity of the Pd nanoparticle catalysts.

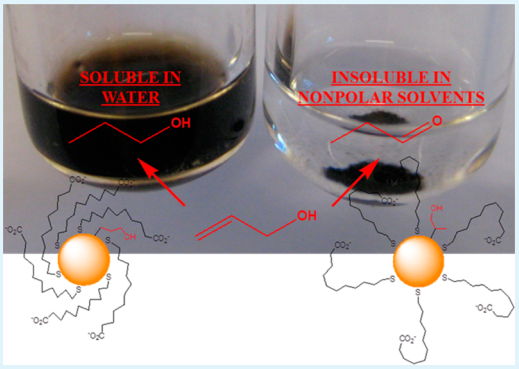

KEYWORDS: *Pd, nanoparticles, allyl alcohol, water-soluble, hydrogenation, isomerization*

INTRODUCTION

During the last two decades, research efforts in the field of metallic nanoparticles has intensified significantly.[1−3] This is due to their vast potential applications in disciplines expanding from electronics,[4,5] optics,[3] sensors,[6−8] and chemical catalysis.[2,9−11] It has been well documented that metal nanoparticles have novel chemical and physical properties compared to those of their bulk counterparts.[12] For example, the high surface atom to volume ratio of materials in nanoscale is often the basis for the high catalytic activities of small metal nanoparticles.[13]

Metal nanoparticles used in catalysis application are, in most cases, fixed onto a surface of solid supports by either intermolecular forces[14,15] or mechanical forces.[16,17] The advantages of these supported catalytic systems include a facile separation of catalysts from the reaction products and a high recyclability with the increased stability.[18] However, the solid-supported heterogeneous catalytic systems usually suffer from the decrease in catalytic activity owing to the kinetic limitations of supported nanoparticles.[19] Furthermore, studies have shown that the surface chemistry provided by the solid supports might have an unpredictable and sometimes undesirable impact on the catalytic activity of metal nanoparticles.[20] Therefore, the homogeneous catalysis based on the principle of diffusion has recently drawn more interest as regards to its potential as a catalytic system with higher activity and selectivity.[21,22]

Current issues associated with homogeneous catalytic application of metal nanoparticles soluble in organic solvents arise from the pollution impact related to the use of toxic organic solvents,[23,24] leaching of delicate core metals,[25] and imperfect recycling.[26] For instance, embracing green chemistry has led to the exploration of nanoparticle catalysts synthesized through biological methods.[27,28] Moreover, a wide variety of ligand stabilizers, such as dendrimers,[10,29−31] polymers,[32] and strongly binding ligands, such as thiols,[33] have been devised to

Received: August 20, 2013
Accepted: November 18, 2013
Published: November 18, 2013

prevent nanoparticle agglomeration or core dissolution to increase stability and amplify recovery during the catalytic reactions. Furthermore, the use of water as a solvent in catalysis is a tactic currently being sought for the application of nanomaterials in green catalysis.[34−36] Some recent examples include semi-natural cellulose-stabilized Pd nanoparticles for the selective hydrogenation of acetylene,[37] olelate-capped Pt nanoparticles for dehalogenation of aryl halide,[38] and thiolate-capped Pd nanoparticles for Suzuki cross-coupling reaction.[39]

In our previous studies, the synthesis of catalytic dodecanethiolate-stabilized palladium nanoparticles (C12PdNP) was achieved by employing sodium *S*-dodecanethiosulfate (Bunte salt) as a ligand precursor.[40] Because of the lower reactivity of sodium *S*-dodecanethiosulfate compared to dodecanethiol during nanoparticle passivation, the metal core size and ligand surface coverage could be efficiently controlled by simply varying reactant equivalents and reaction temperature.[41] Nanoparticle variants consisted of lower surface ligand density and larger core diameters exhibited high catalytic activities.[41,42] Moreover, it was demonstrated that the selectivity of these C12PdNP catalysts could be controlled by varying the polarity of the reaction solvent.[43] The steric effects resulted from the interactions between the hydrophobic/hydrophilic solvent and the highly nonpolar dodecanethiolate ligands managed to direct the selectivity of the hydride insertion, thereby, the structure of Pd-alkyl intermediate.

In this study, two-phase synthesis of water-soluble Pd nanoparticles (ws-PdNP) was attempted with the application of functionalized ligands (sodium ω-carboxyl-*S*-alkanethiosulfates) rather than its nonpolar counterpart in our two-phase thiosulfate synthetic protocol for C12PdNP.[39] The control over this synthesis was further explored by varying the amounts of reactants and the chain length of thiosulfate ligand precursors. Furthermore, the catalytic properties of these unsupported ws-PdNP in the reactions of allyl alcohol in both homogeneous (water) and heterogeneous (chloroform) conditions were studied to obtain further insights into the roles of solvent polarity and ligand structure on the activity and selectivity of the nanoparticle catalysts.

EXPERIMENTAL SECTION

Materials. The following materials were purchased from the indicated suppliers and used as received: Potassium tetrachloropalladate(II) (K_2PdCl_4), tetra-*n*-octylammonium bromide (TOAB), sodium borohydride ($NaBH_4$), 6-bromohexanoic acid, 11-bromoundecanoic acid, and prop-2-en-1-ol (allyl alcohol) were purchased from ACROS. $CDCl_3$ and D_2O were purchased from Cambridge Isotope Laboratories. Sodium thiosulfate ($Na_2S_2O_3\cdot 5H_2O$), toluene, acetone, acetonitrile, methanol, ethanol, chloroform, and tetrahydrofuran (THF) were obtained from Fisher Scientific. Spectra/Por cellulose ester (CE) dialysis membranes (MW = 8000−10 000 Da) were purchased from Spectrum Laboratories, Inc. Water was purified by Barnstead NANOpure Diamond ion exchange resins purification unit.

Synthesis of Sodium ω-Carboxyl-*S*-Alkanethiosulfate Ligands. ω-Carboxyl-*S*-undecanethiosulfate sodium salt was prepared according to the following procedure. In a 500 mL round-bottom flask, 11-bromoundecanoic acid (25 mmol) in 50 mL of ethanol and sodium thiosulfate pentahydrate (25 mmol) in 50 mL of water were mixed. The reaction mixture was refluxed for 3 h, and the solvents were removed by rotary evaporation. The crude product was dissolved in hot ethanol and recrystallized overnight resulting in pure sodium ω-carboxyl-*S*-undecanethiosulfate. ^{1}H NMR (400 MHz, D_2O): δ 3.07 (t, 2H, $C\underline{H}_2S_2O_3^-$), δ 2.34 (t, 2H, $C\underline{H}_2CO_2^-$), δ 1.72 (m, 2H, $C\underline{H}_2CH_2S^-$), δ 1.57 (m, 2H, $C\underline{H}_2CH_2CO_2^-$), δ 1.37−1.27 (m, 12H, $C\underline{H}_2$). IR: 1717 cm^{-1} (C═O stretch), 2923−2912 cm^{-1} (C−H sp^3 stretch), 3300−2800 cm^{-1} (O−H stretch) (Supporting Information Figures S1 and S2).

The synthetic procedure is analogous for sodium ω-carboxyl-*S*-hexanethiosulfate with the exception of the starting material of 6-bromohexanoic acid. ^{1}H NMR (400 MHz, D_2O): δ 3.13 (t, 2H, $C\underline{H}_2S_2O_3^-$), δ 2.43 (t, 2H, $C\underline{H}_2CO_2^-$), δ 1.80 (m, 2H, $C\underline{H}_2CH_2S^-$), δ 1.66 (m, 2H, $C\underline{H}_2CH_2CO_2^-$), δ 1.47 (m, 2H, $C\underline{H}_2$). IR: 1725 cm^{-1} (C═O stretch), 2938−2878 cm^{-1} (sp^3 C−H stretch), 3300−2800 cm^{-1} (O−H stretch) (Supporting Information Figures S3 and S4).

Synthesis of ω-Carboxylate-*S*-Alkanethiolate-Capped Pd Nanoparticles. The following synthesis is similar to a standard procedure using sodium *S*-dodecanethiosulfate, which was introduced in our previous work.[40] Reaction conditions, which were systematically varied, were as follows: (1) the thiosulfate ligand precursors (sodium ω-carboxyl-*S*-hexanethiosulfate or sodium ω-carboxyl-*S*-undecanethiosulfate); (2) the amount of thiosulfate ligand precursors; and (3) the amount of $NaBH_4$.

K_2PdCl_4 (0.40 mmol) was dissolved in 12 mL of nanopure water and TOAB (2.0 mmol) was dissolved in 25 mL of toluene. Both solutions were mixed and continuously stirred until the organic layer turned dark orange and the aqueous layer became clear, indicating the completion of the phase transfer of $PdCl_4^{2-}$. The aqueous layer was discarded and the organic layer was placed in a 250 mL round-bottom flask. ω-Carboxyl-*S*-alkanethiosulfate sodium salt (0.80 mmol) dissolved in 10 mL of 25% methanol was added to the organic layer; additional TOAB (2.0 mmol) was then added to the reaction flask. The reaction mixture was continuously stirred for 15 min. Afterwards, $NaBH_4$ (8.0 mmol) in 7 mL of nanopure water vortexed for ∼10 s was rapidly delivered to the vigorously stirred mixture using a ceramic Hirsh funnel for a continuous delivery. Consequently, the solution darkened immediately, indicating the formation of nanoparticles. Upon the completion of 3 h stirring, the organic layer was discarded by using a separatory funnel (this process was omitted for PdNPs synthesized from ω-carboxyl-*S*-undecanethiosulfate because of the partitioning of PdNPs in both the aqueous and organic layers), and the solvent was removed by rotary evaporation. The resulting crude nanoparticles were suspended in 25 mL of methanol (acetone for PdNPs synthesized from ω-carboxyl-*S*-undecanethiosulfate) and poured down onto a coarse funnel frit (F). The PdNPs were then further washed with several aliquots of methanol, ethanol, THF, chloroform, acetonitrile, and acetone (only methanol, acetonitrile and acetone for PdNPs synthesized from ω-carboxyl-*S*-undecanethiosulfate). The resulting nanoparticles were dissolved in water and placed in dialysis tubes overnight. Afterwards, the water was removed by rotary evaporation and the nanoparticles were dried in vacuum overnight at a pressure of 25 psi.

Catalytic Hydrogenation of Allyl Alcohol. Catalysis experiments were performed by placing 3 mL of D_2O or $CDCl_3$ along with 5 mol % PdNP catalysts in a 100 mL glass round-bottom flask equipped with a rubber stopper. This solution was purged with H_2 gas for 10 min. After the influx of H_2 gas was stopped, 50 μL of allyl alcohol was injected into the sealed reaction flask. The reaction was continuously stirred at room temperature for the predetermined time. An aliquot of the solution was quickly transferred to a NMR tube to obtain ^{1}H NMR spectra.

Instruments. ^{1}H NMR spectra were obtained on a Bruker AC400 FT-NMR spectrometer operating at 400 MHz using the residual solvent peaks as a reference. FT-IR spectra were obtained using a Perkin Elmer Spectrum 100 FT-IR spectrometer. UV−vis spectra from 900 to 300 nm were obtained using a Shimadzu UV-2450 UV-Spectrometer. Transmission electron microscope (TEM) images were obtained with a JEOL 1200 EX II electron microscope operating at a 90 keV. Samples were prepared by placing 10 μL of PdNP aqueous solution (∼1 mg/mL) on a 200 mesh copper grid with formvar film (Ted Pella carbon type B). Size distribution analysis of PdNP microscope images was executed with Scion Image Beta Release 2. Background subtraction was done by Rolling Ball at a set radius of 25. Measurement options were done by Ellipse Major Axis. Thermogravimetric analysis (TGA) was conducted using a TA Instruments SDT

Scheme 1. Reaction Scheme for the Two-Phase Synthesis of Water-Soluble Palladium Nanoparticles Generated from ω-Carboxyl-S-alkanethiosulfate Salts

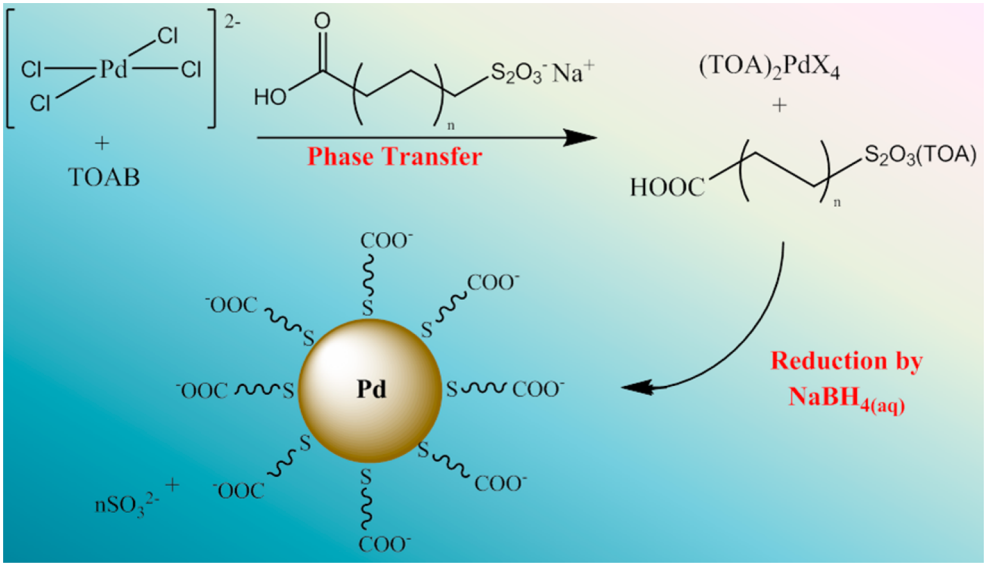

Q600 with a flow rate of 100 mL/min of N_2 with heating from room temperature to 600 °C.

RESULTS AND DISCUSSION

Synthesis of Water-Soluble Pd Nanoparticle (ws-PdNP) Catalysts. Following the success of our prior studies in investigating the synthetic control and catalytic application of dodecanethiolate-capped PdNPs (C12PdNP), the synthesis of water-soluble 11-mercaptoundecanoic acid-capped PdNP (ws-MUA-PdNP) with the similar ligand chain length as that of C12PdNP was attempted. ws-MUA-PdNPs have previously been synthesized by directly employing 11-mercaptoundecanoic acid as a ligand.[39,44] Although MUA-PdNPs have recently been used for the model Suzuki cross-coupling reaction in catalysis application,[39] these nanoparticles are generally not recognized as efficient catalysts for chemical reactions because of the formation of densely packed MUA ligands and subsequent poisoning of the catalyst surfaces.

The synthesis of ws-MUA-PdNP, which involved employing sodium ω-carboxyl-S-undecanethiosulfate as a ligand precursor, began with the phase transfer of $PdCl_4^{2-}$ to an organic layer by TOAB (Scheme 1). Upon completion of the phase transfer, indicated by the appearance of clear aqueous layer, the ω-carboxyl-S-undecanethiosulfate salt was added along with additional TOAB to ensure the full transfer of thiosulfate ligand precursor to the organic layer. The addition of $NaBH_4$ led to the reduction of Pd^{2+} to Pd^0, followed by the nucleation and growth of Pd atoms to nanosized particles. The ws-MUA-PdNP was generated after the assembly of thiosulfate ligands on the nanoparticle surface and the ensuing cleavage of sulfite moiety.[40,45−50]

According to our prior studies, TOAB, the phase transfer agent, is critical for the formation of catalytically active nanoparticles species; the positively charged surfactant is capable of hindering the rapid ligand passivation by the kinetically slow alkanethiosulfates.[40] In addition, ^{1}H NMR studies revealed that the water-soluble ω-carboxyl-S-undecanethiosulfate ligands were actually hydrolyzed to its thiolate or disulfide counterpart by D_2O-sodium borohydride in one-phase system (Supporting Information Figure S5). Since thiolate ligands exhibit a higher reactivity during the nucleation−growth-passivation step than the thiosulfate ligand counterparts, PdNPs generated from a single aqueous phase exhibited no catalytic activity in association with their overall high surface ligand density. Therefore, by employing a biphasic synthetic system, we were able to exploit the benefits of the less reactive thiosulfate functionality.

The presence of a carboxylate group along with the long alkyl chain in the MUA ligands caused the produced PdNP crudes to be temporary soluble in both aqueous and organic phases. Upon the removal of both solvents and extensive washing to eradicate free ligands and surfactants, the isolated MUA-PdNP fully fostered its water solubility. The ws-MUA-PdNP was then placed in dialysis tubes for the removal of ionic salt impurities. Prolonged dialysis of ws-MUA-PdNP (longer than 16 h) caused the partial aggregation of PdNPs and was avoided.

Appropriately, the spectrometric analysis of the ws-MUA-PdNP was accomplished by FT-IR, ^{1}H NMR, and UV−vis spectroscopy measurements. As shown in Supporting Information Figure S6, the IR results confirmed the presence of CH_3/CH_2 stretches at 3000−2850 cm^{-1} along with the peaks corresponding to carboxylate groups at 1550 cm^{-1} and 1400 cm^{-1} ($\nu_{as}CO_2^-$; strong and $\nu_sCO_2^-$; strong, respectively) and carboxylic acid groups at ∼3300 cm^{-1} (ν_sO−H; broad). The ^{1}H NMR spectra of MUA-PdNP (Supporting Information Figure S7) displayed rather broad resonances located at δ 2.13, δ 1.51, δ 1.36, and δ 1.25 for CH_2 groups. This broadening of resonances suggested that the ligands are attached to the nanoparticle and experience the peak-broadening effects as do monolayers of alkanethiolate-protected nanoparticles. The absence of additional peaks corresponding to other water-soluble organic impurities such as sodium ω-carboxyl-S-undecanethiosulfate (Supporting Information Figure S2) and Pd species was another important supporting data for the thiolate monolayer formation and the high purity of Pd nanoparticles. The UV−vis spectra (Supporting Information Figure S8) of ws-MUA-PdNP showed an exponential decay in absorbance with a decrease in energy, which is a feature of typical PdNP with no evident surface plasmon.[40] UV−vis

results also confirmed the absence of the absorption bands corresponding to both Pd(II) species and oxidized Pd.

TEM image of ws-MUA-PdNP shown in Figure 1 resembles that of typical ligand-stabilized nanoparticles, which are

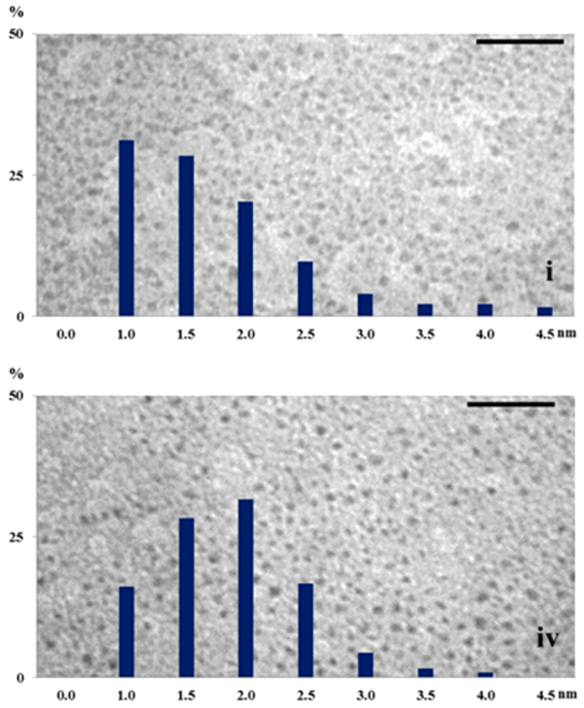

Figure 1. TEM images and size histograms of ws-MUA-PdNP (**i**) and (**iv**) generated from sodium ω-carboxyl-*S*-undecanethiosulfate: (**i**) ws-MUA-PdNP generated from the standard condition and (**iv**) MUA-PdNP generated from three fourths sodium borohydride compared to the standard condition (**i**). Scale bars are 20 nm. Histograms document at least 500 counts.

spherical and without any evidence of aggregation.[40,41] Using the magic numbers based on theoretical models of nanoparticle truncoctahedron geometry[51] and the obtained average core size from TEM results, the ligand surface coverage was calculated from palladium and organic weight percentages of nanoparticles (Table 1). Because the synthetic conditions for ws-MUA-PdNP

Table 1. Systematic Variations Applied to the Synthesis of ws-PdNPs (i–iv, MUA-PdNPs; v, MHA-PdNP) along with Characterization Results[a]

NP catalyst	ligand	$NaBH_4$	TGA (% Pd)	TEM[b] (dia, nm)	ligands/surface atoms[c]
C12PdNP[d]	2	20	68.6	2.40 ± 1.15	0.52
i	2	20	60.7	1.72 ± 0.83	0.50
ii[e]	<2	20			
iii[e]	2	10			
iv	2	15	66.5	1.83 ± 0.68	0.39
v	2	20	75.0	1.69 ± 0.87	0.38

[a]The equivalent values of ligand and $NaBH_4$ are against one equivalent of K_2PdCl_4. Ten equivalent of TOAB were used for all reactions. [b]Average core size was calculated from the histogram analysis of TEM images. [c]Ligand surface coverage calculations were based surface atoms of theoretical models of a truncoctahedron geometry of a certain metal core size and organic weight percentages.[50] [d]Dodecanethiolate-capped PdNP generated from sodium *S*-dodecylthiosulfate reported in ref 41. [e]This condition led to insoluble agglomerated PdNP crudes.

(**i**) were analogous to that of C12PdNP, the comparison seen in the first two entries in Table 1 between **i** and C12PdNP provided some limited insights into the effects of the carboxylate functionality during the nucleation-passivation stage of the synthesis. It appears that the increased kinetic activity of more polar ω-carboxyl-*S*-undecanethiosulfate ligands in toluene caused the metal core size of ws-MUA-PdNP (**i**) to be substantially reduced. Nevertheless, the magnitude of surface ligand coverage was nearly same as that of the hydrophobic correspondent.

Our previous work using sodium *S*-alkanethiosulfate as a ligand precursor demonstrated that the systematic variation of the reaction parameters during the synthesis of PdNPs allowed further control in the surface ligand density of palladium nanocatalysts and an optimization of their catalytic activity and selectivity.[41] The formation of optimized PdNPs with a high degree of colloidal stability in organic solvents required the adjustments in the amount of thiosulfate ligands, TOAB, and $NaBH_4$ and also the reaction temperature. The similar optimization of ws-MUA-PdNP catalysts was attempted by varying the amount of thiosulfate ligands and reducing agents and the hydrophobic chain length of ω-carboxyl-*S*-alkanethiosulfate ligands. The amount of TOAB and the reaction temperature have been optimized according to the standard condition (Table 1, **i**) used in the previous publication.[41]

The initial variation attempted was a decrease in the concentration of the precursor ligand, sodium ω-carboxyl-*S*-undecanethiosulfate, from 2 to 1 equivalent. The decreased amount of the thiosulfate ligand precursor was to provide less ligand stabilizers during the nucleation–growth stage, thereby, generating nanoparticles with the lower surface ligand coverage and likely the larger average core size as reported in our previous publication.[41] However, this attempt only produced a nanoparticle crude that was insoluble in water, indicating a lack of stabilizing ligands during the passivation step and an uncontrollable growth of NPs resulting in the formation of unusable agglomerated product (Table 1, **ii**).

The investigation continued with analyzing the effects of decrease in the amount of reducing agent, $NaBH_4$, during the NP synthesis. In principle, a lower amount of reducing agent should cause the activation of fewer Pd^0 seeds during the initial nucleation stage. The variation involving a 10-fold molar equivalents of reducing agent (Table 1, **iii**), which is one-half of the standard reaction condition used for the catalyst (**i**), produced the agglomerated NP crude during the reaction. Such results were consistent with a lower activation of seeds causing some uncontrolled growth of NP core during the nanoparticle nucleation. However, the moderate 25% decrease in the amount of $NaBH_4$ was able to avoid this problem and yielded stable ws-MUA-PdNP (Table 1, **iv**). While the MUA-PdNP (**iv**) had only slight increase in average core size compared to the ws-MUA-PdNP (**i**) as shown in Figure 1, the calculated surface ligand density was clearly lower (Table 1, **iv**) than that of the ws-MUA-PdNP (**i**). It is believed that the decreased amount of $NaBH_4$ increases the amount of active tetraoctylammonium surfactants (by forming less $TOA^+BH_4^-$ complex) that can effectively compete with the thiosulfate ligands during the nanoparticle ligand passivation.

Since ws-MUA-PdNPs are composed of polar hydrophilic external anionic groups and hydrophobic inner shells, the configuration highly resembles a micelle structure.[52] Therefore, modifying the hydrophobic chain length would provide an interesting option of manipulating the size of these

unimolecular micelle nanostructures. The synthetic procedure for the water-soluble 6-mercaptohexanoic acid-capped Pd nanoparticles (ws-MHA-PdNP) stands analogous to that of the ws-MUA-PdNP as discussed earlier. However, the shorter hydrophobic chain length made the sodium ω-carboxyl-*S*-hexanethiosulfate ligand comparably more polar and increased the solubility of the produced NPs in an aqueous environment compared to its MUA counterpart. Such property was clearly demonstrated in the synthesis after the borohydride reduction of the Pd^{2+} precursor. Upon the nanoparticle formation, unlike the ws-MUA-PdNP, the ws-MHA-PdNP situated itself fully in the aqueous layer leaving the organic layer completely clear. In this case, the removal of the toluene layer from the two-phase reaction mixture, now possible, eliminated the majority of organic impurities such as TOAB from the crude product. The subsequent dialysis of ws-MHA-PdNP in water removed residual salts and excess water-soluble ligand precursors from the PdNPs. The ws-MHA-PdNP variation (Table 1, **v**), synthesized with the standard conditions identical to the ws-MUA-PdNP (**i**), boasted an average metallic core with a diameter of 1.69 nm (Figure 2). This is almost identical to the

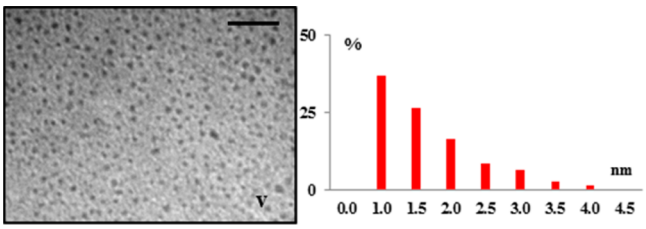

Figure 2. TEM image and size distribution histogram of ws-MHA-PdNP (**v**) generated from sodium ω-carboxyl-*S*-hexanethiosulfate. Scale bars are 20 nm. Histograms document at least 500 counts.

average core size of its counterpart ws-MUA-PdNP (**i**). The metal core size along with its organic content of the variation (**v**) showed that this ws-MHA-PdNP conferred a much lower ligand surface coverage than the ws-MUA-PdNP (**i**) synthesized under the same reaction condition. This is likely due to some partitioning of the highly water-soluble ω-carboxyl-*S*-hexanethiosulfate into the aqueous layer during the addition of aq. $NaBH_4$ solution, decreasing the concentration of the thiosulfate ligands in organic layer. Further characterizations involving variation (**v**) with IR, ^{1}H NMR, and UV−vis spectroscopy revealed similar evidential features to those of ws-MUA-PdNPs (Supporting Information Figures S11−S13).

Catalytic Hydrogenation/Isomerization of Allyl Alcohol Using Water-Soluble Pd Nanoparticles. The catalytic properties of the ws-MUA-PdNP (**i** and **iv**) and the ws-MHA-PdNP (**v**) were tested for the reaction of allyl alcohol in both homogeneous condition (D_2O) and heterogeneous condition ($CDCl_3$) as shown in Table 2.

According to the resulting turnover frequencies, the ws-MUA-PdNP (**i**) clearly outperformed the hydrophobic **C12PdNP** for the reaction in aqueous media. Although the overall surface ligand coverage of both nanoparticle catalysts was of similar magnitude, the benefits of a uniform homogeneous system as compared to the heterogeneous one ultimately caused the observed difference in catalytic activity. When applying $CDCl_3$ as a solvent in the catalytic system, the hydrophobic **C12PdNP** dissolved, while the MUA-PdNP (**i**) remained insoluble in the non-polar solution. In this case, **C12PdNP** in homogeneous condition was clearly more reactive than ws-MUA-PdNP (**i**) in heterogeneous system. The contrast regarding the selectivity toward the catalytic isomerization was clearly noticeable: a 95% conversion compared to 12% in a four hour reaction time for **C12PdNP** and (**i**), respectively. The additional ws-MUA-PdNP variant (**iv**) featured a lower surface ligand density (Table 1) and displayed a much higher catalytic activity than ws-MUA-PdNP (**i**) in both homogeneous and unsupported heterogeneous systems. Because of its increased catalytic execution, the effects of employing distinct solvent polarities were far more apparent. In D_2O, the allyl alcohol substrate was fairly selectively converted to its hydrogenation product, 1-propanol (58% yield). When $CDCl_3$ was utilized as solvent in the reaction system, the ws-MUA-PdNP variation (**iv**) catalyzed the reactant more towards the isomerization product, propanal (64% yield). Scheme 2 graphically represents the solvent dependent catalytic selectivity of this ws-MUA-PdNP (**iv**).

In our previous studies, the solvent dependent catalytic selectivity of **C12PdNP** has been demonstrated.[43] The mechanistic studies suggested that the π-coordination of the allyl alcohol substrate to Pd−H rich surface was followed by the formation of a Pd-alkyl intermediate. Ultimately, the selectivity of reaction for either isomerization or hydrogenation products depended on the regioselective insertion of the Pd−H to the C=C bond (Scheme 3). As evidenced by our experimental results, the hydrophobic dodecanethiolate ligands readily

Table 2. Catalytic Performance of ws-MUA-PdNP (i/iv) and ws-MHA-PdNP (v) with 5 mol % Pd and 5 mmol H_2 Gas in the Reaction of Allyl Alcohol

			catalysis yields (%)				
NP catalyst	solvent	reaction time (h)	allyl alcohol	1-propanol	propanal	Hyd. TOF[a]	Iso. TOF[a]
C12PdNP[b]	D_2O	24	35	48	17	40	14
	$CDCl_3$	4	0	5	95	25	475
i	D_2O	4	64	33	3	165	15
	$CDCl_3$	4	73	15	12	75	60
iv	D_2O	4	31	58	11	290	55
	$CDCl_3$	4	20	16	64	80	320
v	D_2O	4	4 (0)[c]	91 (98)[c]	5 (2)[c]	455 (490)[c]	25
	$CDCl_3$	4	82	9	9	45	45

[a]Turnover frequencies (initial TOFs) of fresh PdNPs (5 mol % in Pd atoms) are based on the mole reacted per mol Pd atoms per hour. [b]The results of catalytic reactions with dodecanethiolate-capped Pd nanoparticles generated from sodium *S*-dodecylthiosulfate reported in ref 43. [c]The yields in parentheses are obtained from the catalytic reaction of allyl alchol using 10 mmol H_2 gas.

Scheme 2. Catalytic Selectivity by Water-Soluble Palladium Nanoparticle Catalysts in the Hydrogenation/Isomerization of Allyl Alcohol in Homogeneous (D_2O) and Heterogeneous ($CDCl_3$) Conditions

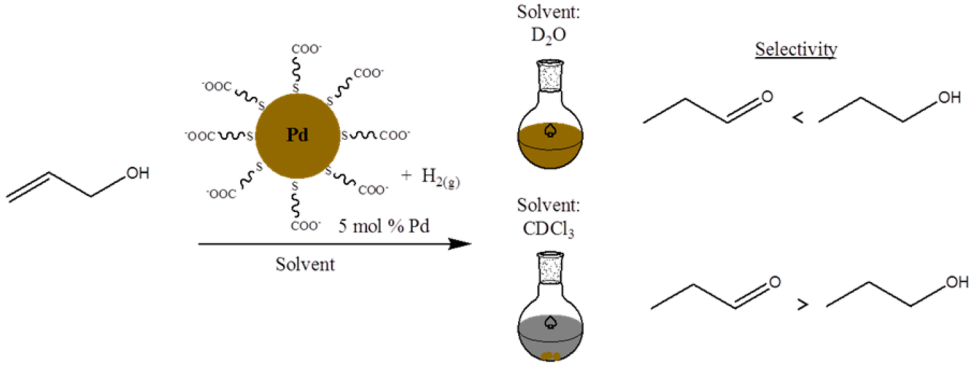

Scheme 3. Mechanism of Hydrogenation/Isomerization of Allyl Alcohol Using Palladium Nanoparticles Catalysts

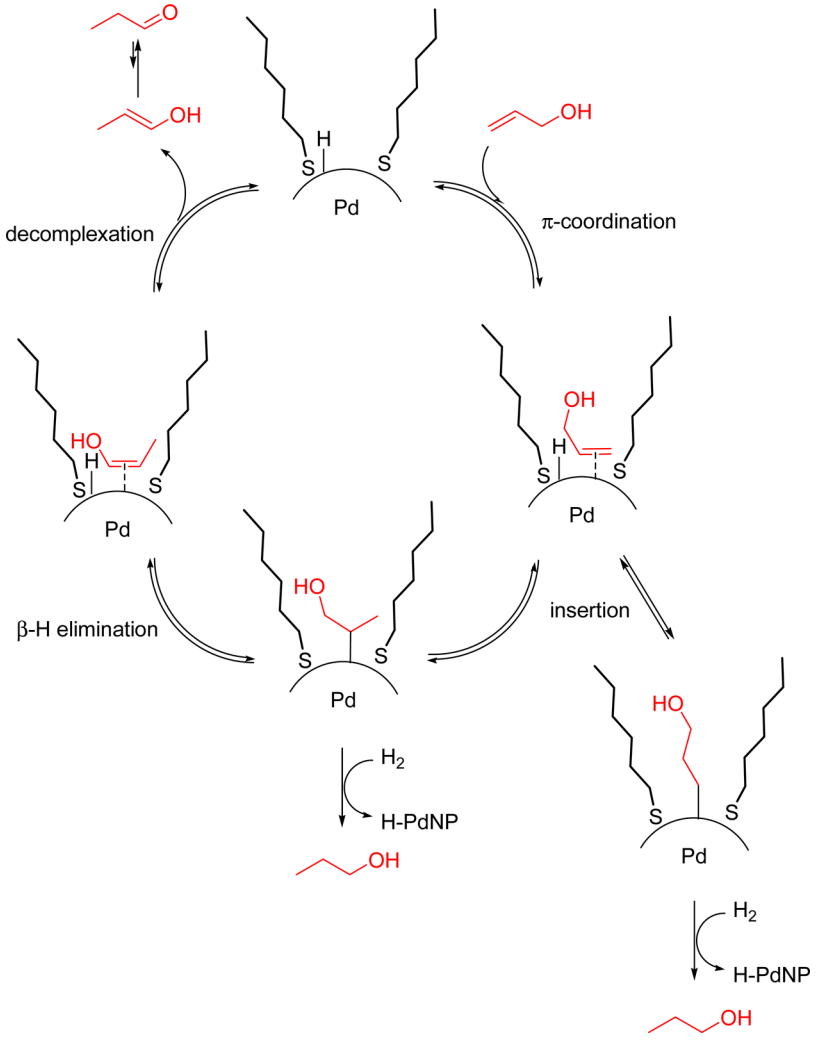

undergo swelling when exposed to nonpolar organic solvents, thus, generating a fully extended ligand conformation. Such conformation provided the least amount of steric hindrance by the dodecanethiolate ligands during the insertion step, thereby allowing for the formation of a branched Pd-alkyl (Markornikov addition) intermediate and promoting the isomerization of allyl alcohol to propanal (Scheme 3, β-elimination). As for the reaction in D_2O, the immobilized dodecanethiolate ligands collapsed on to the nanoparticle surface in order to decrease interactions with polar protic solvent, D_2O. This conformation, unlike the prior, affords the higher steric interference to the palladium core causing the preferable formation of a linear Pd-alkyl (anti-Markornikov addition) intermediate and promoting the hydrogenation of allyl alcohol to 1-propanol (Scheme 3).

Although the solubility of the ws-MUA-PdNP (**iv**) is opposite to that of the **C12PdNP**, the preceding principles are still applicable to this catalytic system. The carboxylate functionality of MUA-ligand residing at the ligand end point,

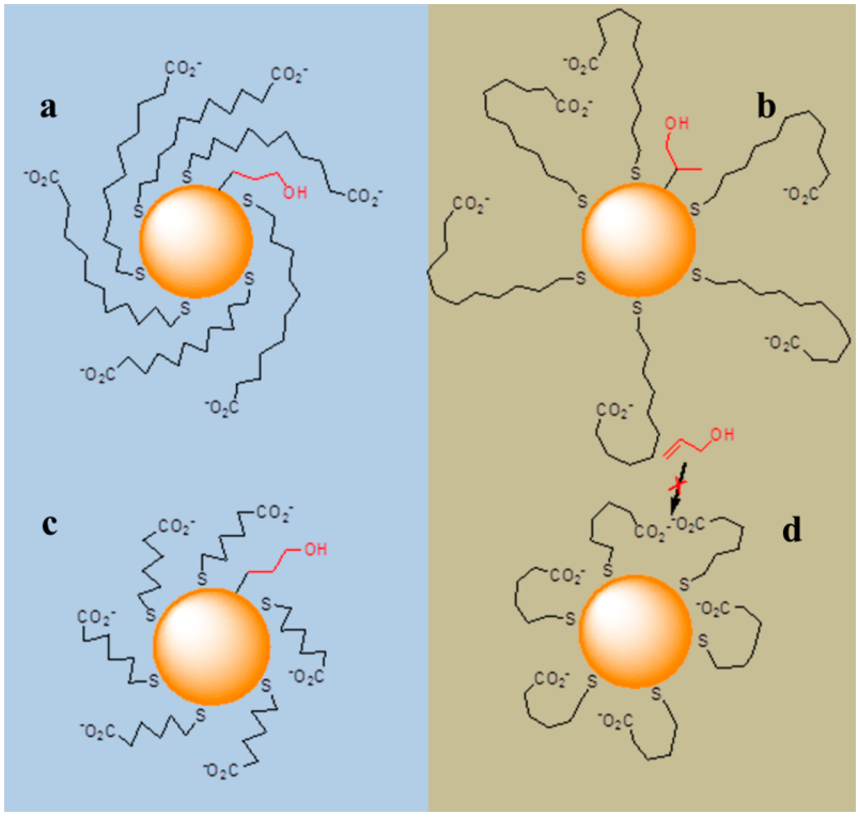

Figure 3. Proposed conformations of the ligands on Pd nanoparticles and the structure of Pd-alkyl intermediates: (a) ws-MUA-PdNP in D_2O, (b) ws-MUA-PdNP in $CDCl_3$, (c) ws-MHA-PdNP in D_2O, and (d) ws-MUA-PdNP in $CDCl_3$.

farthest away from the catalytic sites located at the PdNP surface, made the nanoparticles to be soluble in aqueous environments. Nevertheless, the hydrophobic chemical environment at the ws-PdNP surface is quite similar to that of **C12PdNP**. Within that regard, the physical structure of these ws-PdNPs resembled that of colloidal surfactant packed aggregates, known as micelles. However, these ligand-capped metal nanoparticles are unique unimolecular suprastructures with immobilized hydrophobic alkyl chains. Therefore, their structural integrity regarding the overall density of the hydrophobic alkyl chains is higher than that of micelles. As a consequence, the conformation of hydrophobic chains around the nanoparticle core mostly depends on the polarity of surrounding solvent molecules. When dissolved in D_2O, the MUA-chains are likely collapsed toward the PdNP surface, while the hydrophilic carboxylate are still capable of solvating the nanoparticle. The resulting compact structure of surrounding ligands increases the steric hindrance for the formation of the branched Pd-alkyl intermediate and favors the generation of the linear Pd-alkyl intermediate (Figure 3a), increasing selectivity for the hydrogenation product (1-propanol).

On the other hand, the repulsion between the hydrophilic carboxylate groups of MUA-PdNPs and the nonpolar solvent, $CDCl_3$, causes these ws-PdNP catalysts to aggregate and appear insoluble. Interestingly, the comparison between the unsupported heterogeneous catalytic system in $CDCl_3$ and the homogeneous condition in D_2O indicated that the catalytic activities of ws-MUA-PdNP (**iv**) in two different reaction conditions are unexpectedly similar, indicated by similar TOF values. On the basis of the catalytic selectivity and kinetics results, it is believed that the MUA-chains of the ws-PdNP remain ascent after the partial swelling by the nonpolar $CDCl_3$ solvent, thereby, leaving an active PdNP surface open for the faster reaction. This is especially important for the more catalytically active ws-PdNP (**iv**), which has a lower surface ligand coverage than the ws-PdNP (**i**) as shown in Table 1. The ascent ligand conformation and the lower surface ligand coverage of ws-MUA-PdNP (**iv**) in $CDCl_3$ was capable of allocating enough near-surface space for the formation of a branched Pd-alkyl intermediate, henceforth, favoring the isomerization product (Figure 3b).

Lastly, the catalytic properties of the ws-MHA-PdNP (**v**) were also assessed in both homogeneous and heterogeneous reaction conditions (Table 2). The homogeneous reaction in D_2O was the most effective for the catalytic hydrogenation of allyl alcohol performed in this study, yielding over 91% of 1-propanol. The good catalytic activity of this nanocatalyst could be accounted for its possession of the lower surface ligand coverage and the shorter ligand chain length. The formation of linear Pd-alkyl intermediate was more favorable because of the steric hindrance associated with the immobilized alkyl chains, therefore highly favoring the hydrogenation product (Figure 3c). The MHA-PdNP (**v**) with good catalytic selectivity towards hydrogenation was further tested in catalytic reaction of allyl alcohol in D_2O under the increased amount of hydrogen gas (10 mmol). The increase in H_2 gas concentration resulted in a higher reaction conversion indicated by the absence of allyl alcohol along with the rise in yields of 1-propanol to 98% (Table 2).

In contrast, a poor activity was attained when applying $CDCl_3$ as a solvent during heterogeneous catalysis. This result was rather expected based on our unimolecular micelle model of these catalysts. By employing a shorter hydrophobic chain, the external hydrophilic carboxylate groups are more stuffed

towards the Pd surface in hydrophobic $CDCl_3$ solvents. The surface immobilized ligands with this conformation crafts ligand barriers, in which substrates and even solvent molecules have difficulty in penetrating between the ligands (Figure 3d). Furthermore, given the similar average metal core size and ligand surface coverage between the ws-PdNP catalysts (**iv**) and (**v**), the increase in the catalytic hydrogenation of allyl alcohol in D_2O and the higher selectivity to 1-propanol by the catalyst (**v**) should be inferred because of the difference in alkyl chain lengths of surrounding ligands on these two particles (Figure 3). Specifically, the shorter alkyl chain of the MHA-PdNP (**v**) provided much less steric hindrance for the adsorption of allyl alcohol on PdNP surfaces compared to the longer alkyl chain of the MUA-PdNP (**iv**).

The possibility of other factors affecting the selectivity of the reaction, such as the direct involvement of D_2O molecules and the leaching of PdNP during the reaction, has been investigated for the MHA-PdNP (**v**). The involvement of D_2O in the catalytic reaction, which was examined by monitoring the incorporation of deuterium to the final product in the NMR spectra, was not observed. This eliminated the possibility of solvent providing extra surface H on to Pd surfaces and the formation of Pd-D adduct during the reaction. UV−vis results of the reaction mixture also confirmed the absence of the absorption bands corresponding to both Pd(II) species during the catalytic reactions in both D_2O and $CDCl_3$.

To examine the stability of water-soluble catalysts, the MHA-PdNP (**v**) was isolated from the homogeneous solution after the catalytic reaction. The methanol-induced precipitation followed by the subsequent centrifugation and decantation of reaction mixtures were performed. The precipitates were re-dissolved in water for characterization by TEM (Supporting Information Figure S15) and UV−vis spectroscopy (Supporting Information Figure S16). TEM results showed the high population of small MHA-PdNP without any significant size and morphological changes. UV−vis results also confirmed the absence of the absorption bands corresponding to Pd(II) species. The previous report from our group has also shown the high recyclability of dodecanethiolate-capped Pd nanoparticles from the same reactions in organic solvents.[43]

CONCLUSIONS

The synthesis of stable water-soluble palladium nanoparticles was achieved by utilizing sodium ω-carboxyl-*S*-alkanethiosulfate as ligand precursors. Although the systematic variations of the synthetic parameters proved to be somewhat limited compared to the synthetic conditions applied to hydrophobic alkanethiolate-capped Pd nanoparticles, these water-soluble palladium nanoparticles catalysts were fairly successful in hydrogenation of allyl alcohol in water. The results also demonstrated that the catalytic activity and selectivity of these palladium nanoparticles were influenced by not only the ligand surface coverage and ligand chain length of Pd nanoparyticles but also the thiolate monolayer conformation that was largely controlled by the interaction between monolayers and surrounding solvent environments.

ASSOCIATED CONTENT

Supporting Information

^{1}H NMR and FT-IR results of sodium ω-carboxyl-*S*-undecanethiosulfate and sodium ω-carboxyl-*S*-hexanethiosulfate. ^{1}H NMR, FT-IR, and UV-vis spectroscopy results and TGA results of ws-MUA- and ws-MHA-Pd nanoparticles. TEM and UV−vis spectroscopy results of ws-MHA-Pd nanoparticles after catalysis reaction. This material is available free of charge via the Internet at http://pubs.acs.org.

AUTHOR INFORMATION

Corresponding Author

*E-mail: ys.shon@csulb.edu. Tel: 562-985-4466. Fax: 562-985-8547.

Notes

The authors declare no competing financial interest.

ACKNOWLEDGMENTS

This research was supported in part by grants from the ACS-PRF (PRF49407-UR7), National Institutes of General Medical Science (SC3GM089562), and CSULB (MGSS and RSCA awards).

REFERENCES

(1) Chaudhuri, R. G.; Paria, S. *Chem. Rev.* **2012**, *112*, 2373−2433.
(2) Roy, S.; Pericàs, M. A. *Org. Biomol. Chem.* **2009**, *7*, 2669−2677.
(3) Cortie, M. B.; McDonagh, A. M. *Chem. Rev.* **2011**, *111*, 3713−3735.
(4) Bakr, O. M.; Amendola, V.; Aikens, C. M.; Wenseleers, W.; Li, R.; Dal Negro, L.; Schatz, G. C.; Stellacci, F. *Angew. Chem., Int. Ed.* **2009**, *48*, 5921−5926.
(5) Soreta, T. R.; Strutwolf, J.; Henry, O.; O'Sullivan, C. K. *Langmuir* **2010**, *26*, 12293−12299.
(6) Lin, H.-Y.; Chen, C.-T.; Chen, Y.-C. *Anal. Chem.* **2006**, *78*, 6873−6878.
(7) Lin, S.-Y.; Liu, S.-W.; Lin, C.-M.; Chen, C.-H. *Anal. Chem.* **2002**, *74*, 330−335.
(8) McNicholas, T. P.; Zhao, K.; Yang, C.; Hernandez, S. C.; Mulchandani, A.; Myung, N. V.; Deshusses, M. A. *J. Phys. Chem. C* **2011**, *115*, 13927−13931.
(9) Malkov, A.V.; Figlus, M.; Cooke, G.; Caldwell, S. T.; Rabani, G.; Prestly, M. R.; Kočovsky, P. *Org. Biomol. Chem.* **2009**, *7*, 1878−1883.
(10) Crooks, R. M.; Zhao, M.; Sun, L.; Chechik, V.; Yeung, L. K. *Acc. Chem. Res.* **2001**, *34*, 181−190.
(11) Scholten, J. D.; Caroline, B.; Dupont, J. *ACS Catal.* **2012**, *2*, 184−200.
(12) Zhang, J. Z.; Wang, Z.-L.; Liu, J.; Chen, S.; Liu, G.-Y. *Self-Assembled Nanostructures*; Kluwer Academic/Plenum Publishers: New York, 2002.
(13) Astruc, D. *Transition-Metal Nanoparticles in Catalysis: From Historical Background to the State-of-the Art, in Nanoparticles and Catalysis*; Astruc, D., Ed.; Wiley-VCH Verlag GmbH & Co. KGaA: Weinheim, Germany, 2008.
(14) Kim, J.; Chung, Y.-M.; Kang, S.-M.; Choi, C.-H.; Kim, B.-Y.; Kwon, Y.-T.; Kim, T. J.; Oh, S.-H.; Lee, C.-S. *ACS Catal.* **2012**, *2*, 1042−1048.
(15) Higgins, D. C.; Meza, D.; Chen, Z. *J. Phys. Chem. C* **2010**, *114*, 21982−21988.
(16) Liang, X.; Li, J.; Yu, M.; McMurray, C. N.; Falconer, J. L.; Weimer, A. W. *ACS Catal.* **2011**, *1*, 1162−1165.
(17) Wunder, S.; Polzer, F.; Lu, Y.; Mei, Y.; Ballauff, M. *J. Phys. Chem. C* **2010**, *114*, 8814−8820.
(18) Wu, P.; Loh, K. P.; Zhao, X. S. *Sci. Adv. Mater.* **2011**, *3*, 970−983.
(19) Ono, F.; Kanemasa, S.; Tanaka, J. *Tetrahedron Lett.* **2005**, *46*, 7623−7626.
(20) Grirrane, A.; Corma, A.; Garcia, H. *J. Catal.* **2009**, *264*, 138−144.
(21) Astruc, D.; Lu, F.; Aranzaes, J. R. *Angew. Chem., Int. Ed.* **2005**, *44*, 7852−7872.
(22) Semagina, N.; Kiwi-Minsker, L. *Catal. Rev.* **2009**, *51*, 147−217.

(23) El Badawy, A. M.; Silva, R. G.; Morris, B.; Scheckel, K. G.; Suidan, M. T.; Tolaymat, T. M. *Environ. Sci. Technol.* **2011**, *45*, 283−287.
(24) Yinghuai, Z.; Chenyan, K.; Peng, A.T.; Emi, A.; Monalisa, W.; Louis, L.K.-J.; Hosmane, N.S.; Maguire, J.A. *Inorg. Chem.* **2008**, *47*, 5756−5761.
(25) Ananikov, V. P.; Beletskaya, I. P. *Organometallics* **2012**, *31*, 1595−1604.
(26) Moshfegh, A. Z. *J. Phys. D: Appl. Phys.* **2009**, *42*, 233001.
(27) Huang, J.; Wang, W.; Lin, L.; Li, Q.; Lin, W.; Li, M.; Mann, S. *Chem. Asian J.* **2009**, *4*, 1050−1054.
(28) Gardea-Torresdey, J. L.; Parsons, J. G.; Gomez, E.; Peralta-Videa, J.; Troiani, H. E.; Santiago, P.; Yacaman, M. J. *Nano Lett.* **2002**, *2*, 397−401.
(29) Myers, V. S.; Weir, M. G.; Carino, E. V.; Yancey, D. F.; Pande, S.; Crooks, R. M. *Chem. Sci.* **2011**, *2*, 1632−1646.
(30) Scott, R.W. J.; Wilson, O. M.; Oh, S.-K.; Kenik, E. A.; Crooks, R. M. *J. Am. Chem. Soc.* **2004**, *126*, 15583−15591.
(31) Huang, W.; Kuhn, J. N.; Tsung, C.-K.; Zhang, Y.; Habas, S. E.; Yang, P.; Somorjai, G.A. *Nano Lett.* **2008**, *8*, 2027−2034.
(32) Metin, Ö.; Özkar, S. *Energy Fuels* **2009**, *23*, 3517−3526.
(33) Eklund, S. E.; Cliffel, D. E. *Langmuir* **2004**, *20*, 6012−6018.
(34) Zhu, F.-X.; Wang, W.; Li, H.-X. *J. Am. Chem. Soc.* **2011**, *133*, 11632−11640.
(35) Sharghi, H.; Khalifeh, R.; Doroodmand, M. M. *Adv. Synth. Catal.* **2009**, *351*, 207−218.
(36) Caporali, M.; Guerriero, A.; Caporali, S.; Ienco, A.; Peruzzini, M.; Gonsalvi, L. *ChemCatChem.* **2013**, *5*, 2517−2526.
(37) Zhang, H.; Yang, Y.; Dai, W.; Yang, D.; Lu, S.; Ji, Y. *Catal. Sci. Technol.* **2012**, *2*, 1319−1323.
(38) Xu, S.; Yang, Q. *J. Phys. Chem. C* **2008**, *112*, 13419−13425.
(39) Cargnello, M.; Wieder, N. L.; Canton, P.; Montini, T.; Giambastiani, G.; Benedetti, A.; Gorte, R. J.; Fornasiero, P. A *Chem. Mater.* **2011**, *23*, 3961−3969.
(40) Sadeghmoghaddam, E.; Lam, C.; Choi, D.; Shon, Y.-S. *J. Mater. Chem.* **2011**, *21*, 307−312.
(41) Gavia, D.J.; Shon, Y.-S. *Langmuir* **2012**, *28*, 14502−14508.
(42) Gavia, D.J.; Koeppen, J.; Sadeghmoghaddam, E.; Shon, Y.-S. *RSC Adv.* **2013**, *3*, 13642−13645.
(43) Sadeghmoghaddam, E.; Gu, H.; Shon, Y.-S. *ACS Catal.* **2012**, *2*, 1838−1845.
(44) Cargnello, M.; Wieder, N. L.; Montini, T.; Gorte, R. J.; Fornasiero, P. *J. Am. Chem. Soc.* **2010**, *132*, 1402−1409.
(45) Lukkari, J.; Meretoja, M.; Kartio, I.; Laajalehto, K.; Rajamäki, M.; Lindström, M.; Kankare, J. *Langmuir* **1999**, *15*, 3529−3537.
(46) Shon, Y.-S.; Gross, S. M.; Dawson, B.; Porter, M.; Murray, R. W. *Langmuir* **2000**, *16*, 6555−6561.
(47) Shon, Y.-S.; Cutler, E. *Langmuir* **2004**, *20*, 6626−6630.
(48) Mari, A.; Imperatori, P.; Marchegiani, G.; Pilloni, L.; Mezzi, A.; Kaciulis, S.; Cannas, C.; Meneghini, C.; Mobilio, S.; Suber, L. *Langmuir* **2010**, *26*, 15561−15566.
(49) Lohse, S. E.; Dahl, J. A.; Hutchison, J. E. *Langmuir* **2010**, *26*, 7504−7511.
(50) Fealy, R. J.; Ackerman, S. R.; Ferguson, G. S. *Langmuir* **2011**, *27*, 5371−5376.
(51) Hostetler, M. J.; Wingate, J. E.; Zhong, C.-J.; Harris, J. E.; Vachet, R. W.; Clark, M. R.; Londono, J. D.; Green, S. J.; Stokes, J. J.; Wignall, G. D.; Glish, G. L.; Porter, M. D.; Evans, N. D.; Murray, R. W. *Langmuir* **1998**, *14*, 17−30.
(52) Mai, Y.; Eisenberg, A. *Acc. Chem. Res.* **2012**, *45*, 1657−1666.